Surface and micromechanical analysis of polyurethane plates with hydroxyapatite for bone structure

Wenderson da Silva do Amaral[1] , Milton Thélio de Albuquerque Mendes[1] ,
João Victor Frazão Câmara[2]* , Josué Junior Araujo Pierote[3] , Fernando da Silva Reis[4] ,
José Milton Elias de Matos[4] , Ana Cristina Vasconcelos Fialho[1] and Walter Leal de Moura[1]

[1]Departamento de Patologia e Clínica Odontológica, Centro de Ciências da Saúde, Universidade Federal do Piauí, Teresina, Brasil

[2]Klinik für Zahnerhaltung, Parodontologie und Präventivzahnmedizin, Universitätsklinikum des Saarlandes, Homburg, Saar, Deutschland

[3]Universidade Santo Amaro, São Paulo, Brasil

[4]Departamento de Química, Centro de Ciências da Natureza, Universidade Federal do Piauí, Teresina, Brasil

*jvfrazao92@hotmail.com

Abstract

To analyze the surface topography and mechanical properties of a polyurethane derived from castor oil reinforced with hydroxyapatite (PU–HA) for bone fixation. The surface analysis was performed by Scanning Electron Microscopy (SEM) and the mechanical properties by Vickers microhardness and tensile tests. The SEM images showed that the PU surface presented important characteristics for materials intended for bone fixation, such as an irregular and porous surface. The analysis showed a surface with alternating areas with depressions and elevations of approximately 80 ± 100 μm, presence of pores of 12 μm in size. The microhardness analysis showed values of 0.42 ± 1.01 HV for PU–HA plates, lower in relation to the poly lactic-co-glycolic acid (PLGA) plate (control group). The elastic modulus and ultimate tensile strength of 317.4 MPa, and 35.57 MPa for PLGA sample, 1.187 MPa, and 0.29 MPa for PU–HA sample. The PU produced showed good surface properties, however demands better mechanical properties.

Keywords: biocompatible materials, castor oil, fractures, bone.

1. Introduction

Bone fracture fixation with metal plates and screws (titanium, stainless steel, and Fe-Cr-Ni-Mo alloys) represents the gold standard because these materials present high rigidity and strength, helping to keep approximate bone fragments in a safe and stable position[1]. However, disadvantages, such as not following bone growth in pediatric patients, have encouraged the development of fixation systems with resorbable materials.

Resorbable systems are mainly used in pediatric patients in the bone growth phase because resorption occurs over time, usually from six to eight weeks. These materials are indicated for clinical use, promoting surfaces with gradual osteoconductive properties[2]. However, resorbable devices have limitations, such as high cost, the possibility of fracture, the development of foreign body-type reactions, and material-specific complications, including the need for a wider dissection due to the size of devices and complications in molding the plates in the desired shape[1,2].

In this sense, biopolymers of plant origin have been used for developing products to the biomedical field, including

polyurethane[3-8]. Polyurethane from castor oil is a compound that consists of a prepolymer and a polyol extracted from the seed oil of the Ricinus communis plant, which does not exude toxic vapors and is a biocompatible material[9,10].

The amount and composition of the isocyanate and polyol used in the synthesis directly affect polyurethane properties and such material can be prepared for specific applications by varying parameters such as length, distribution of flexible and rigid segments, molar mass, and degree of branching or crosslinking of chains[11]. For a safe clinical application, polyurethane must have a rigidity that allows an internal fixation with an initial force that meets the biomechanical needs. Besides roughness and porosity, some characteristics are relevant for bone fixation devices[12]. This study highlights the use of hydroxyapatite (HA), a bioactive and osteoconductive component for developing bioactive materials that simulate bone tissue composition. Such simulation occurs because of the chemical and structural similarities to the mineral phase of vertebrate bones and teeth[3], inducing bone tissue growth due to a porous structure similar to the porous bone[4].

Thus, the present study aimed to analyze surface topography and mechanical performance of polyurethane from castor oil with hydroxyapatite, intended as a bone fixation material.

2. Materials and Methods

2.1 Polyurethane preparation

The production method followed the protocol by Moura et al.[12]. The composite production sequence occurred at the Material Physics Laboratory of the Federal University of Piauí (Fismat/UFPI). After preparing monoacylglycerol (MAG) from castor oil, it was mixed for polymerization with hexamethylene-1, 6-diisocyanate (1,6 - HDI, Sigma-Aldrich Brasil Ltda™) and poly (ethylene glycol) (PEG) in the proportion of 30% relative to MAG mass, at a controlled temperature and time (the stoichiometric ratio of monomers MAG: 1,6-HDI = 3:1). Hydroxyapatite (HA) was gradually added to the mixture until obtaining PU-HA at a 3% concentration. In the "gel point" phase, the mixture was deposited and closed in a bipartite rectangular container (mold). PEG (62000-6400) was used as a plasticizing agent to improve the mechanical and surface properties of the polymer[13].

2.2 Fourier-Transform Infrared (FTIR) spectroscopy

The FTIR spectra for the synthesized materials were obtained in a Thermo Fisher SCIENTIFIC spectrophotometer, model Nicolet iS5, with a purge pump, wavelength between 400 cm^{-1} and 4000 cm^{-1}, in a transmittance module.

2.3 Scanning electron microscopy

Micrographs were captured in a scanning electron microscope with a field emission gun, brand FEI, model Quanta FEG 250, with accelerating voltage from 1 to 30 kV, and equipped with SDD EDS (Silicon drift detectors), brand Ametek, model HX -1001, Apollo X-SDD detector. The conditions (energy, spot, and magnification) are recorded at the bottom of each photo as scale and magnification (Notation: SE - ETD-SE secondary electron detector).

The samples were fixed on an aluminum substrate (stub) using double-sided carbon adhesive tape, grounded with carbon paint, and coated with Au in a metallizer, Quorum, model Q150R, for 30 seconds at 20 mA, with plasma generated in an argon atmosphere. The micrographs were treated with ImageJ software (open source, free), considering the algorithms used by Paulo et al.[14] and Johner and Meireles[15].

2.4 Vickers microhardness

The samples, in triplicate, were analyzed in a micro-vicker ISH-TDV2000 automatic digital microhardness tester from the mechanical testing laboratory of the Federal University of Piauí at a load of 10 gf. Five measurements were taken in different areas from each of the analyzed samples, as standardized by the ASTM E92 (Standard Test Method for Vickers Hardness and Knoop Hardness of Metallic Materials) and the ASTM E384 (Standard Test Method for Microindentation Materials).

2.5 Mechanical traction test

The samples were analyzed in a universal mechanical testing machine, model Emic DL20000, trd cell 24, and analyzed in Tesc 3.04 software to determine the mechanical properties of the material. The study evaluated the parameters of elasticity, ultimate tensile strength, and deformation at which the materials were analyzed in the equipment at a continuous speed of 10 mm/min.

2.5.1 Statistical analysis

The descriptive analytical statistical analysis was performed with Bioestat™ open source software, version 5.3, at 95% CI and p<0.05.

3. Results and Discussions

3.1 Characterizations

The composition of the produced polyurethane (PU) was confirmed by analyzing the infrared spectra (Figure 1). The transmittance band in the 3315 cm^{-1} region is compatible with the presence of N-H bonds of urethanes and stretching in the 2939 cm^{-1} and 2852 cm^{-1} regions related to asymmetric and symmetric CH$_3$ stretching, respectively. A stretch band at 1700 cm^{-1} corresponding to the carbonyl functional group (C=O), a CO-O bond (urethane) corresponding to the band at 1250 cm^{-1}, and a hydroxyapatite (HA) phosphate radical peaking at 1150 cm^{-1} are compatible with the molecular structure of a castor oil PU composite with HA.

3.2 Topographic surface analysis

The photomicrographs obtained at different magnifications (Figure 2A-2C) show the sample surface characteristics, with porosity areas, projections, depressions, and granular structures distributed across the viewing area in the micrograph. The darker zones represent low areas such as pores and depressions, and the lighter ones represent granulation or surface projection areas. The histogram shows that the highest pixel concentrations are between 50 and 123, peaking at 106, demonstrating a homogeneous distribution between high and low areas of the castor oil-based polymer surface (Figure 2D-2E).

The "Interactive 3D Surface Plot - Spectrum LUT" algorithm allowed the reproduction of the castor oil-based
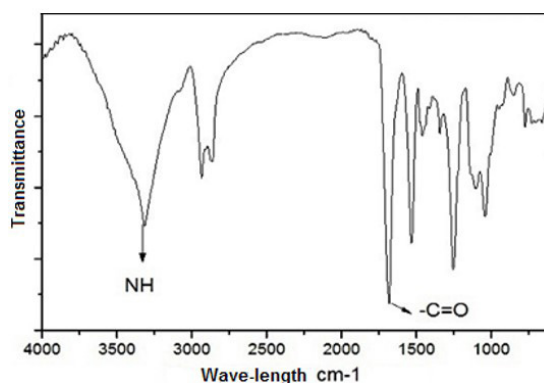
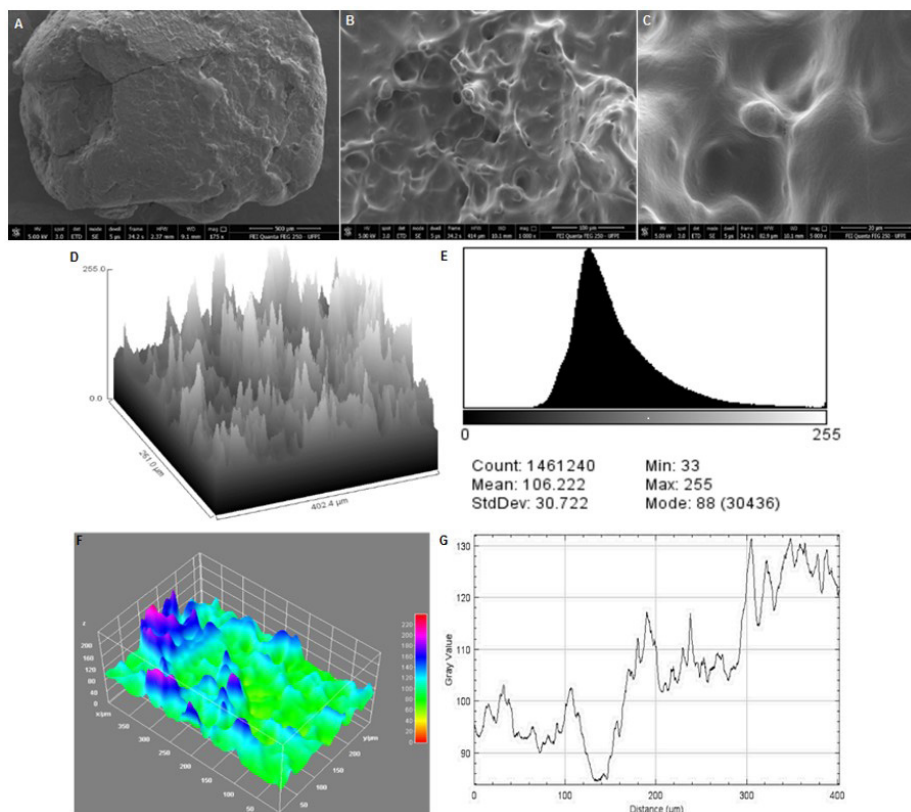**Figure 1.** Infrared spectra (FTIR) of castor based polyurethane.

Figure 2. (A) Photomicrograph of the surface of the PU sample at magnification 175x; (B) 1000x; (C) 5000x; (D) image manipulated using the "Surface Plot" algorithm (ImageJ®); (E) image produced with application of the Histogram algorithm (ImageJ®); (F) image manipulated using ImageJ® software; (G) distribution of pixel values as a function of surface space using ImageJ® software.

PU surface in a 3D image, considering the color variation associated with low and high areas of the analyzed sample surface. The three-dimensional reconstruction (Figure 2F) revealed the alternation between peak regions (blue to red color areas) representing high surfaces and valley regions (green to red colors) representing low areas such as depressions, fissures, and pores. Figure 2G represents the graph produced with the "Plot" algorithm of ImageJ™ software, explaining the distribution of pixel values according to the total surface space of micrograph 10b. The lowest area value is close to 80 μm, and the highest value is close to 130 μm, showing little difference between these regions.

Figure 3A represents the photomicrograph of a porous surface area. This image was treated with the "Interactive 3D Surface Plot" algorithm, which allowed visualizing the depth level of this structure based on the values of pixels represented in a color range. Yellow is the deepest observable point of the pore (40 μm), considering that the surface area circumscribed to the edge differs between high and low structures of approximately 80 to 100 μm.

The ImageJ circular algorithm, followed by commands "Analyze>measure", calculated the mean perimeter of depression and pore areas recorded in the images (Figure 3C). Measurements were performed in four flatter areas, and Bioestat 5.3 calculated the mean of these records. The 3D reconstruction (Figure 3B and 3D) shows blue areas representing

the pores and low texture regions and the reddish or orange areas illustrating greater superficial height.

Moreover, there was a crack on the polymer surface in an image magnified at 500x, and 3D reconstruction showed its path across the sample surface (Figure 4A). The histogram (Figure 4B) shows that the highest pixel values are between 80 and 100, presenting little difference between them and a surface with little differences between the lowest and highest areas. Regarding the crack path (Figure 4C), a depth of around 40 μm was reconstructed in 3D, represented by the yellow color. The histogram (Figure 4D) corresponds to the mean of 73 pixels.

3.3 Mechanical properties

Microhardness was analyzed on samples of castor oil PU and PLGA plates (Inion™) sold commercially (Control group). The analysis was performed by calculating the diagonals of the impression produced with the microdurometer indenter. Student's t-test was applied to two independent samples with unequal variances, in which $p < 0.05$ suggests a statistically significant difference between the mean microhardness values for the analyzed samples (Table 1).

The PLGA samples supported 317 Mega Pascal (MPa) before undergoing irreversible deformation and failed under an applied load of 183 Newtons (N), with approximately
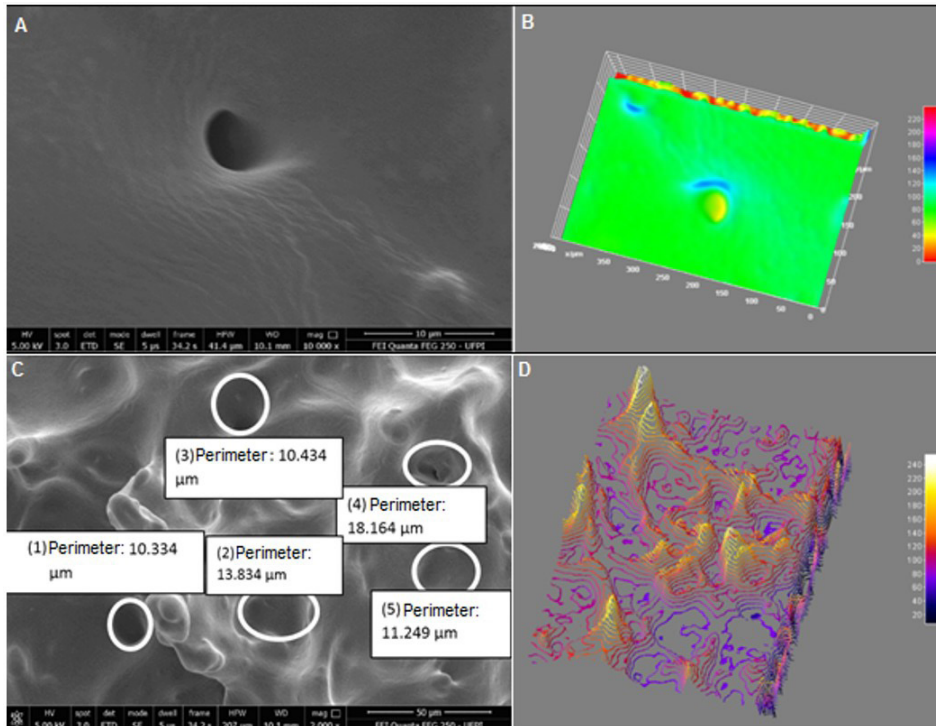
Figure 3. (A) Photomicrograph with 10000x magnification of a porous area of castor based polymer; (B) 3D reconstruction; (C) photomicrograph with analysis of perimeter measurements of circular areas treated by ImageJ software in a 2000x image; and (D) 3D reconstruction set to Isoline.
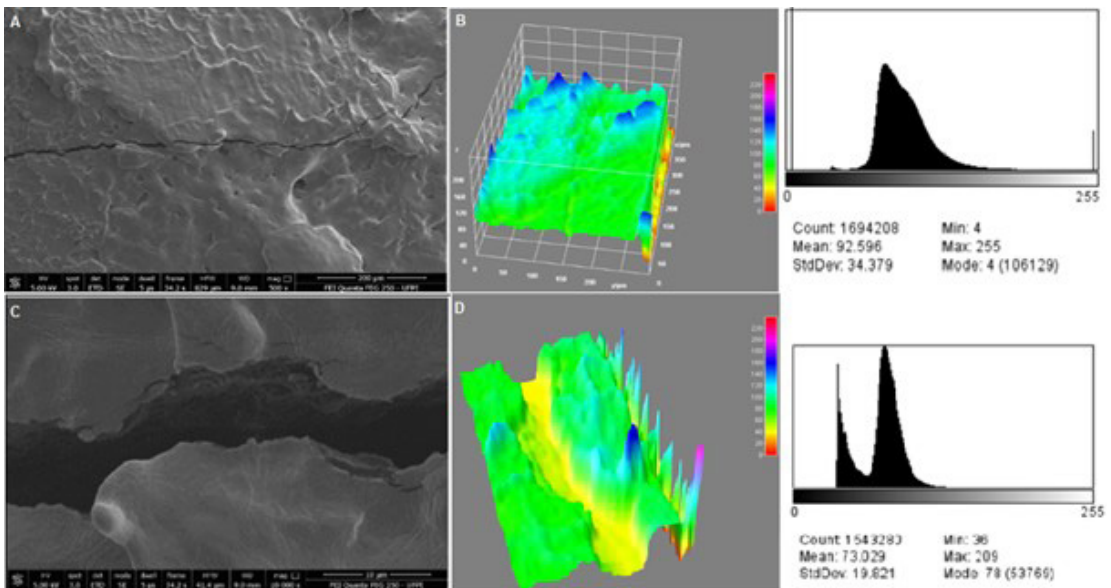

Figure 4. (A) Photomicrograph of the surface of the PU sample showing a crack at a magnification of 500x; (B) 3D reconstruction from the "Interactiv Surface Plot" algorithm (ImageJ®) and histogram with pixel distribution values; (C) photomicrograph of the surface of the sample of PU showing a crack at 10000x magnification; (D) 3D reconstruction using ImageJ® software and pixel histogram.

25% of their structure deformed. For castor oil-based PU, the elastic modulus was 1.19 MPa, and it fractured under an applied load lower than 1 N. Considering that failure occurred at low values, there was no record of a specific strain value for this sample. Thus, the value differences indicated in the graphs show that castor oil-based PU could not withstand the required loads for a bone fixation material, considering that the control sample (PLGA) was used as

Table 1. Vickers microhardness test result for PLGA and PU - HA samples, expressed in vickers number.

PLGA			Polyurethane		
Measure	Value	AVE: 21.14	Measure	Value	AVE: 0.79
1	21.49		1	0.94	
2	23.44	S: 1.72	2	1.01	S: 0.27
3	20.21	Max: 23.44	3	0.42	Max: 1.01
4	21.71	Min: 18.85	4	0.59	Mín: 0.42
5	18.85		5	1.01	

PLGA: Poly lactic-co-glycolic acid; AVE: Average; S: Standard deviation.

a parameter for defining properties for the test sample (PU-HA) (Figure 5A). The effect of HA addition resulted in poorer mechanical properties of the composite. Moreover, the Young's modulus (E) value is strongly affected by the magnitude of the porosity in a material and high porosity values may lead to E values close to zero[1-4]. Our results corroborate the findings of Nasrollah *et al.*, in which higher porosity due to HA addition impairs the mechanical properties and consequently reduces strength, which, in turn, favors the potential for increased cell adhesion and proliferation[4]. In this study, the elastic modulus value was lower than that by Nasrollah and collaborators, but the author also reports divergent results from other studies[4].

Stress-strain curves are commonly used to represent material behavior in tensile tests, representing the behavior of PLGA (Figure 5B) and PU-HA (Figure 5C) samples. The absence of a plastic zone in both materials shows that both groups are fragile in a ductility analysis, meaning that they undergo small deformations until rupture but with higher resistance of the PLGA plate than the PU-HA.

Several types of isocyanates are used for PU production, such as toluene diisocyanate (TDI)[16], dicyclohexylmethane diisocyanate (HMDI)[17], and isophorone diisocyanate[18]. This study used hexamethylene diisocyanate (HDI, Sigma-Aldrich Brasil Ltda™), an aliphatic molecular chain isocyanate ($C_8H_{12}O_2N_2$, 168.2 g/mol) with $OCN(CH_2)_6NCO$ structure that is less reactive than other isocyanates, less volatile, less toxic, and with a flexible, linear, and symmetric molecular structure.

Diisocyanates can have different structures, such as aromatic, aliphatic, cycloaliphatic, or polycyclic. The most reported systems in the literature are based on dihydroxylated polyether or polyester and aliphatic diisocyanates[19]. These compounds are responsible for the so-called rigid segment in the PU structure, giving polymers properties such as hardness, shear strength, and elastic modulus in traction and/or compression[20].

Hydroxyapatite (HA) bioceramic was used at a 3% concentration to improve the mechanical properties of PU, considering the vast literature on its biological properties, biocompatibility, biodegradability, osteoconductive, and osseointegrated characteristics[2,17]. The PU was polymerized using monomeric condensation with CO_2 release, responsible for expanding the material during setting and forming reticular areas inside the polymeric structure. The material remained closed with a tray lid in the curing period of 72 hours to reduce this expansion[12].

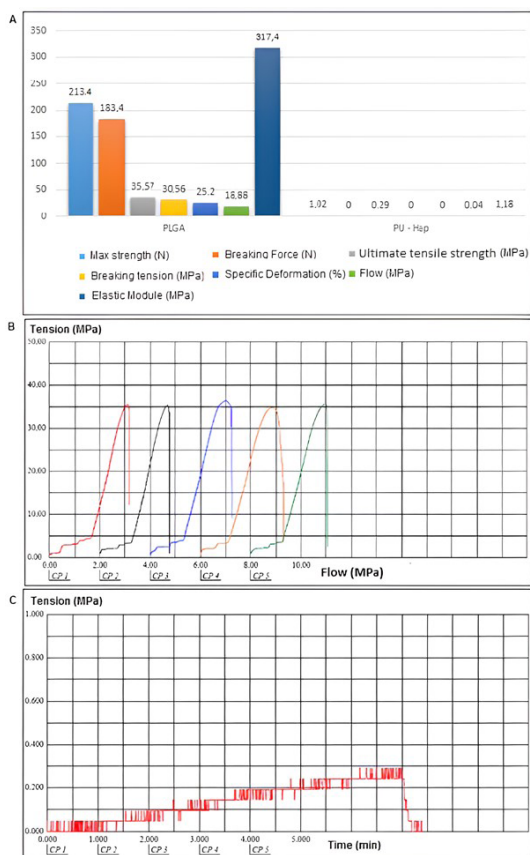Spectroscopy in the infrared region was used because it is the most suitable technique for the qualitative

Figure 5. (A) Tensile test for PLGA board and PU –HA; (B) stress-strain curve for PLGA board; (C) stress-strain curve for PU board –HA.

determination of the products formed, as it is based on the vibrational energies of the bonds in the sample and one of the most important techniques for identifying and/or determining structural characteristics of polymers, especially regarding the functional groups and bonds in the sample[21]. The transmittance band in the 3315 cm⁻¹ region is compatible with the presence of N-H bonds of urethanes and stretching in the 2939 cm⁻¹ and 2852 cm⁻¹ regions related to asymmetric and symmetric CH_3 stretching, respectively. Such results corroborate those by Sathiskumar and Madras[22]. A stretch band at 1700 cm⁻¹ corresponding to the carbonyl functional group (C=O), a CO-O bond (urethane) corresponding to the band at 1250 cm⁻¹, and a hydroxyapatite phosphate radical peaking at 1150 cm⁻¹ are compatible with the molecular

structure of a castor oil-based PU and HA, corroborating the results by Cardoso and Balaban[21].

SEM provided high-resolution images and the amplification of a sample surface. SEM images are three-dimensional and suitable for analyzing and evaluating the surface area of polymer samples[23]. This tool investigates the fracture zone and tries correlating the topographical features of the sample surface[24,25]. Thus, the resulting photomicrographs characterized the surface topography aspects of castor oil-based PU with HA. The images were analyzed with ImageJ™ software algorithms for treating micrographs from electron microscopy. In this software, binary images (8 bits) map grayscale values from 0 (applied to the darkest areas) to 255 (corresponding to the lightest images). Our research group used this technique based on the study by Paulo et al.[14] to visualize the surface topography of a nanoporous alumina membrane. The image treatment performed with the "Interactive 3D Surface Plot - Spectrum LUT" algorithm was also used by Johner and Meireles[15] in their validation study of a production method with image-coupled thin layer chromatography.

The presence of pores on the material surfaces favors a higher physical adhesion between the bone tissue and the fixation system. Hence, the produced castor oil-based PU presents this favorable characteristic for bone fixation[26]. Pore size also affects bone growth. Our study reports approximate pore sizes between 50 and 125 μm, corroborating the findings of Itälä et al.[27].

The fracture observed on the polymer surface had a relatively flat surface, with a fracture pattern called brittle, usual in polymeric bodies. These results were also reported in the study by Rocha et al.[28], which described this fracture type. The method for obtaining the specimens from gel pressing[7] and the presence of solid particles of HA dispersed throughout the internal material structure can explain the irregular and rough material surface. These findings are similar to those by Sousa et al.[29] involving polyhydroxybutyrate membranes with hydroxyapatite. The appearance of cracks on the polymer surface may relate to sample preparation. Pacheco et al.[30] also reported cracks in advanced cementitious composites verified in scanning microscopy images, justifying that this crack is linked to material cutting for analysis.

Material hardness is associated with the capacity to resist elastic deformation, usually by penetration, and is mainly related to atom bonds in material compositions[31]. According to Tan et al.[7], PU from ricinoleic acid has low crosslinking density, hypothesizing the mechanical fragility of our polymer at low microhardness values.

For Gürbüz et al.[32], microhardness can be affected by the type of monomer, filling, morphology, volume, and weight of composites. The values of the different groups show that castor oil-based PU with HA has a lower hardness than the commercially available plate, which implies that the polymer produced at UFPI is more likely to wear and deteriorate. The production technique of specimens is significant for establishing their properties. The method used in this study was compression molding, in which the mold cover was screwed and maintained in place for 72 hours[12].

For Ligowski et al.[33], extrusion is the most suitable method for producing composites. It converts the appropriate raw material into a given product with semi-continuous production in which the material is forced through a matrix, thus acquiring a predetermined shape under controlled conditions. Different authors[34-37] have used this method to produce composites with satisfactory properties, but the literature does not provide comparisons for material properties using other production methods.

According to Callister[31], fragile bodies rupture soon after reaching the proportionality limit, and the plastic phase is virtually non-existent. Thus, the two tested polymers show brittle behavior. The negative sign for flow values indicates contraction and stretching during force application, which is common in such a test performed on polymers. The low polymer value of this parameter is linked to the low deformation resistance of this material[38].

Ductility was analyzed by evaluating the behavior of the stress-strain graphs produced in the test. Fragile bodies undergo reversible deformation proportional to the applied stress up to the breaking point, and ductile bodies undergo reversible deformation up to the proportionality limit but with permanent deformation even after ceasing load application, promoting a plastic behavior that characterizes material ductility[31].

The mixture of two polymers in the PLGA composition (polylactic acid and resorbable trimethylene carbonate copolymer) may explain the resistance of this material[39]. Moreover, the high degree of crystallinity of PLGA provides a high mechanical performance level, unlike the produced PU, which has a semi-crystalline appearance[12]. Tan et al.[7] suggest that the low mechanical performance of the produced PU may also be due to glycerol percentage. In their research, the mechanical properties improved as glycerol concentrations increased, showing their highest module at 60%. In our study, glycerol percentage was 30% relative to MAG mass.

The tensile test also allowed defining the material's ductile or brittle behavior, characterized by the ability to absorb forces before fracture[31]. This is a desirable property for bone fixation devices because, during bone healing, the fracture area receives different forces and must be partially absorbed by the fixation material. Thus, the PU-HA and the PLGA plate showed fragile mechanical behavior, although the PLGA plate performed better than PU.

4. Conclusions

According to our findings, castor oil-based polyurethane with hydroxyapatite showed interesting characteristics required for bone fixation procedure, however regarding the mechanical properties need reassessing.

5. Author's Contribution

• **Conceptualization** – Wenderson da Silva do Amaral; Walter Leal de Moura.

• **Data curation** – Wenderson da Silva do Amaral; Milton Thélio de Albuquerque Mendes.

• **Formal analysis** – Wenderson da Silva do Amaral.

• **Funding acquisition** – Walter Leal de Moura.

• **Investigation** – Wenderson da Silva do Amaral; Fernando da Silva Reis.

• **Methodology** – Wenderson da Silva do Amaral; Ana Cristina Vasconcelos Fialho.

• **Project administration** – Wenderson da Silva do Amaral; José Milton Elias de Matos.

• **Resources** – Wenderson da Silva do Amaral; Josué Junior Araujo Pierote.

• **Software** – Wenderson da Silva do Amaral; Fernando da Silva Reis.

• **Supervision** – Walter Leal de Moura.

• **Validation** – Walter Leal de Moura.

• **Visualization** – Walter Leal de Moura.

• **Writing – original draft** – Wenderson da Silva do Amaral.

• **Writing – review & editing** – João Victor Frazão Câmara; Walter Leal de Moura.

6. References

1. Moghaddaszadeh, A., Seddiqi, H., Najmoddin, N., Ravasjani, S. A., & Klein-Nulend, J. (2021). Biomimetic 3D-printed PCL scaffold containing a high concentration carbonated-nanohydroxyapatite with immobilized-collagen for bone tissue engineering: enhanced bioactivity and physicomechanical characteristics. *Biomedical Materials*, *16*(6), 065029. http://dx.doi.org/10.1088/1748-605X/ac3147. PMid:34670200.

2. Shojaei, B., Abtahi, M., & Najafi, M. (2020). Chemical recycling of PET: a stepping-stone toward sustainability. *Polymers for Advanced Technologies*, *31*(12), 2912-2938. http://dx.doi.org/10.1002/pat.5023.

3. Akhigan, N., Najmoddin, N., Azizi, H., & Mohammadi, M. (2022). Zinc oxide surface-functionalized PCL/graphene oxide scaffold: enhanced mechanical and antibacterial properties. *International Journal of Polymeric Materials and Polymeric Biomaterials*, 1-11. http://dx.doi.org/10.1080/00914037.2022.2100373. Online.

4. Usha, P. G., Jalajakumari, S., Sheela, U. B., Gopalakrishnan, A. M., & Nair, S. T. T. (2022). Polysaccharide nanofibers and hydrogel: a comparativeevaluation on 3D cell culture and tumor reduction. *Journal of Applied Polymer Science*, *139*(43), e53044.

5. Lima, F., Melo, W. G., Braga, M. F., Vieira, E., Câmara, J. V., Pierote, J. J., Argôlo, N. No., Silva, E. Fo., & Fialho, A. C. (2021). Chitosan-based hydrogel for treatment of temporomandibular joint arthritis. *Polímeros: Ciência e Tecnologia*, *31*(2), e2021019. http://dx.doi.org/10.1590/0104-1428.20210026.

6. Heidrich, D., Fortes, C. B. B., Mallmann, A. T., Vargas, C. M., Arndt, P. B., & Scroferneker, M. L. (2019). Rosemary, castor oils, and propolis extract: activity against *Candida Albicans* and alterations on properties of dental acrylic resins. *Journal of Prosthodontics*, *28*(2), e863-e868. http://dx.doi.org/10.1111/jopr.12746. PMid:29322644.

7. Tan, A. C. W., Polo-Cambronell, B. J., Provaggi, E., Ardila-Suárez, C., Ramirez-Caballero, G. E., Baldovino-Medrano, V. G., & Kalaskar, D. M. (2018). Design and development of low cost polyurethane biopolymer based on castor oil and glycerol for biomedical applications. *Biopolymers*, *109*(2), e23078. http://dx.doi.org/10.1002/bip.23078. PMid:29159831.

8. Lima, F. S., Matos, L. F., Pacheco, I. K., Reis, F., Câmara, J. V. F., Pierote, J. J. A., Matos, J. M., Ribeiro, A., Moura, W., & Fialho, A. C. (2022). Scaffold based on castor oil as an osteoconductive matrix in bone repair: biocompatibility analysis. *Polímeros: Ciência e Tecnologia*, *32*(1), e2022003. http://dx.doi.org/10.1590/0104-1428.210018.

9. Ozimek, J., & Pielichowski, K. (2021). Recent advances in polyurethane/POSS hybrids for biomedical applications. *Molecules*, *27*(1), 40. http://dx.doi.org/10.3390/molecules27010040. PMid:35011280.

10. Griffin, M., Castro, N., Bas, O., Saifzadeh, S., Butler, P., & Hutmacher, D. W. (2020). The current versatility of polyurethane three-dimensional printing for biomedical applications. *Tissue Engineering. Part B, Reviews*, *26*(3), 272-283. http://dx.doi.org/10.1089/ten.teb.2019.0224. PMid:32089089.

11. Morais, J. P. P., Pacheco, I. K. C., Maia, A. L. M. Fo., Ferreira, D. C. L., Viana, F. J. C., Reis, F. S., Matos, J. M. E., Rizzo, M. S., & Fialho, A. C. V. (2021). Polyurethane derived from castor oil monoacylglyceride (*Ricinus communis*) for bone defects reconstruction: characterization and in vivo testing. *Journal of Materials Science. Materials in Medicine*, *32*(4), 39. http://dx.doi.org/10.1007/s10856-021-06511-z. PMid:33792773.

12. Moura, F. N. No., Fialho, A. C. V., Moura, W. L., Rosa, A. G. F., Matos, J. M. E., Reis, F. S., Mendes, M. T. A., & Sales, E. S. D. (2019). Castor polyurethane used as osteosynthesis plates: microstructural and thermal analysis. *Polímeros: Ciência e Tecnologia*, *29*(2), e2019029. http://dx.doi.org/10.1590/0104-1428.02418.

13. Fiori, A. P. S. M., Gabiraba, V. P., Praxedes, A. P. P., Nunes, M. R. S., Balliano, T. L., Silva, R. C., Tonholo, J., & Ribeiro, A. S. (2014). Preparação e caracterização de nanocompósitos poliméricos baseados em quitosana e argilo minerais. *Polímeros: Ciência e Tecnologia*, *24*(5), 628-635. http://dx.doi.org/10.1590/0104-1428.1572.

14. Paulo, V. I. M., Neves-Araujo, J., & Padron-Hernandez, E. (2019). Fast and room-temperature synthesis of Porous Alumina films in ultrasonic assisted bath inducing superficial cavitations. *Portugaliae Electrochimica Acta*, *37*(2), 123-129. http://dx.doi.org/10.4152/pea.201902123.

15. Johner, J. C. F., & Meireles, M. A. A. (2016). Construction of a supercritical fluid extraction (SFE) equipment: validation using annatto and fennel and extract analysis by thin layer chromatography coupled to image. *Food Science and Technology*, *36*(2), 210-247. http://dx.doi.org/10.1590/1678-457X.0027.

16. Costa, O. A. P., Petzhold, C. L., Gerbase, A. E., & Silva, R. B. (2017). Síntese e caracterização de compósitos de poliuretanas obtidas com poliol-soja/TDI/cargas minerais. *Revista Virtual de Química*, *9*(4), 1434-1448.

17. Liu, H., Zhang, L., Li, J., Zou, Q., Zuo, Y., Tian, W., & Li, Y. (2010). Physicochemical and biological properties of nano-hydroxyapatite-reinforced aliphatic polyurethanes membranes. *Journal of Biomaterials Science. Polymer Edition*, *21*(12), 1619-1636. http://dx.doi.org/10.1163/092050609X12524778957011. PMid:20537245.

18. Uscátegui, Y. L., Arévalo, F. R., Díaz, L. E., Cobo, M. I., & Valero, M. F. (2016). Microbial degradation, cytotoxicity and antibacterial activity of polyurethanesbased on modified castor oil and polycaprolactone. *Journal of Biomaterials Science. Polymer Edition*, *27*(18), 1860-1879. http://dx.doi.org/10.1080/09205063.2016.1239948. PMid:27654066.

19. Coutinho, F. M. B., Delpech, M. C., Alves, T. L., & Gomes, A. S. (2002). Síntese e caracterização de poliuretanos em dispersão aquosa à base de polibutadieno líquido hidroxilado e diferentes diisocianatos. *Polímeros: Ciência e Tecnologia*, *12*(4), 248-254. http://dx.doi.org/10.1590/S0104-14282002000400007.

20. Clemente, M., Rocha, R. J., Iha, K., & Rocco, J. A. F. F. (2014). Desenvolvimento de tecnologia de pré-polímeros na síntese de poliuretanos empregados em combustíveis sólidos. *Química Nova*, 37(6), 982-988.

21. Cardoso, O. R., & Balaban, R. C. (2013). Preparação de resinas de poliuretana à base de óleo de mamona e dietanolamina e sua aplicação em circuitos eletroeletrônicos. *Polímeros: Ciência e Tecnologia*, 23(4), 552-558. http://dx.doi.org/10.4322/polimeros.2013.003.

22. Sathiskumar, P. S., & Madras, G. (2011). Synthesis, characterization, degradation of biodegradable castor oil based polyesters. *Polymer Degradation & Stability*, 96(9), 1695-1704. http://dx.doi.org/10.1016/j.polymdegradstab.2011.07.002.

23. Erdman, N., Bell, D. C., & Reichelt, R. (2019). *Scanning electron microscopy*. In P. W. Hawkes & J. C. H. Spence (Eds.), *Springer handbook of microscopy* (pp.229-318). Cham: Springer. http://dx.doi.org/10.1007/978-3-030-00069-1_5.

24. Chinaglia, C. R., & Correa, C. A. (1997). Análise de falhas em materiais através de técnicas avançadas de microscopia. *Polímeros: Ciência e Tecnologia*, 7(3), 19-23. http://dx.doi.org/10.1590/S0104-14281997000300005.

25. Pacheco, I. K. C., Reis, F. S., Carvalho, C. E. S., Matos, J. M. E., Argôlo, N. M. No., Baeta, S. A. F., Silva, K. R., Dantas, H. V., Sousa, F. B., & Fialho, A. C. V. (2021). Development of castor polyurethane scaffold (*Ricinus communis* L.) and its effect with stem cells for bone repair in an osteoporosis model. *Biomedical Materials*, 16(6), 065006. http://dx.doi.org/10.1088/1748-605X/ac1f9e. PMid:34416741.

26. Aparecida, A. H., Guastaldi, A. C., & Fook, M. V. L. (2008). Desenvolvimento e caracterização de suportes porosos de polietileno de ultra alto peso molecular (PEUAPM) para utilização como biomaterial para reposição e regeneração óssea. *Polímeros: Ciência e Tecnologia*, 18(4), 277-280. http://dx.doi.org/10.1590/S0104-14282008000400004.

27. Itälä, A. I., Ylänen, H. O., Ekholm, C., Karlsson, K. H., & Aro, H. T. (2001). Pore diameter of more than 100 microm is not requisite for bone ingrowth in rabbits. *Journal of Biomedical Materials Research*, 58(6), 679-683. http://dx.doi.org/10.1002/jbm.1069. PMid:11745521.

28. Rocha, G. B. T., Pereira, L. M. M., Farias, L. D. P., Gandur, N. L., Flores, P. M., Oliveira, R. M., & Silva, M. H. P. (2016). Análise fractográfica em MEV: fratura dúctil x fratura frágil. *Revista Militar de Ciência e Tecnologia, 33*(2), 85-87. Retrieved in 2023, January 18, from https://rmct.ime.eb.br/arquivos/RMCT_4_tri_2016_web/PICM_2016_B3_final.pdf

29. Sousa, W. J. B., Barbosa, R. C., Fook, M. V. L., Filgueira, P. T. D., & Tomaz, A. F. (2017). Membranas de polihidroxibutirato com hidroxiapatita para utilização como biomaterial. *Revista Matéria*, 22(4), e-11902. http://dx.doi.org/10.1590/s1517-707620170004.0236.

30. Pacheco, F., Christ, R., Gil, A. M., & Tutikian, B. F. (2016). SEM and 3D microtomography application to investigate the distribution of fibers in advanced cementitious composites. *Revista IBRACON de Estruturas e Materiais*, 9(6), 824-841. http://dx.doi.org/10.1590/s1983-41952016000600002.

31. Callister, W. D. C. (2007). *Materials science and engineering*. New York: John Wiley & Sons.

32. Gürbüz, Ö., Cilingir, A., Dikmen, B., Ozsoy, A., & Eren, M. A. (2020). Efeito do selante de superfície na rugosidade superficial de diferentes compósitos e avaliação de sua microdureza. *European Oral Research*, 54(1), 1-8. http://dx.doi.org/10.26650/eor.20200020. PMid:32518904.

33. Ligowski, E., Santos, B. C., & Fujiwara, S. T. (2015). Materiais compósitos a base de fibras da cana-de-açúcar e polímeros reciclados obtidos através da técnica de extrusão. *Polímeros: Ciência e Tecnologia*, 25(1), 70-75. http://dx.doi.org/10.1590/0104-1428.1605.

34. Santos, E. F., Moresco, M., Rosa, S. M. L., & Nachtigall, S. M. B. (2010). Extrusão de compósitos de PP com fibras curtas de coco: efeito da temperatura e agentes de acoplamento. *Polímeros: Ciência e Tecnologia*, 20(3), 215-220. http://dx.doi.org/10.1590/S0104-14282010005000036.

35. Oliveira, R. V. B., Ferreira, C. I., Peixoto, L. J. F., Bianchi, O., Silva, P. A., Demori, R., Silva, R. P., & Veronese, V. B. (2013). Mistura polipropileno/poliestireno: um exemplo da relação processamento-estrutura-propriedade no ensino de polímeros. *Polímeros: Ciência e Tecnologia*, 23(1), 91-96. http://dx.doi.org/10.1590/S0104-14282013005000001.

36. Azevedo, J. B., Viana, J. D., Carvalho, L. H., & Canedo, E. L. (2016). Caracterização de compósitos obtidos a partir de polímero biodegradável e casca de arroz utilizando duas técnicas de processamento. *Revista Matéria*, 21(2), 391-406. http://dx.doi.org/10.1590/S1517-707620160002.0037.

37. Erbetta, C. D. C., Viegas, C. C. B., Freitas, R. F. S., & Sousa, R. G. (2011). Syntesis and termal and chemical characterization of the poly (D,L – lactide – co – glycolide). *Polímeros: Ciência e Tecnologia*, 21(5), 376-382. http://dx.doi.org/10.1590/S0104-14282011005000063.

38. Passos, I. A. G., Marques, J. N., Câmara, J. V. F., Simão, R. A., Prado, M., & Pereira, G. D. S. (2022). Effect of non-thermal argon plasma on the shear strength of adhesive systems. *Polímeros: Ciência e Tecnologia*, 32(1), e2022012. http://dx.doi.org/10.1590/0104-1428.20220019.

39. Melo, R. B., Tavares, W. L. B., Fonseca, W. L. M., Silva, D. A. C., Pontes, I. V., & Barbalho, J. C. M. (2015). Utilização de sistema de fixação bioabsorvível em caso de fratura mandibular em paciente pediátrico. *Revista de Cirurgia e Traumatologia Buco-Maxilo-Facial*, 15(2), 45-48. Retrieved in 2023, January 18, from https://www.revistacirurgiabmf.com/2015/2/07-Utilizacaodesistemadefixacaoabsorvivel.pdf